Injection Locking and Parametric Locking in a Superconducting Circuit

Danijela Marković, Jean-Damien Pillet, Emmanuel Flurin, Nicolas Roch, Benjamin Huard

Injection Locking and Parametric Locking in a Superconducting Circuit

D. Marković,[1] J.D. Pillet,[2] E. Flurin,[3] N. Roch,[4] and B. Huard[5,1,*]

[1] *Laboratoire de Physique de l'Ecole Normale Supérieure, ENS, Université PSL, CNRS, Sorbonne Université, Université Paris-Diderot, Sorbonne Paris Cité, Paris, France*

[2] *Laboratoire des Solides Irradiés, École Polytechnique, CNRS, CEA, Palaiseau 91128, France*

[3] *SPEC, CEA, CNRS, Université Paris-Saclay, CEA Saclay, Gif-sur-Yvette 91191, France*

[4] *Université Grenoble Alpes, CNRS, Grenoble INP, Institut Néel, 25 rue des Martyrs, BP 166, Grenoble, 38042, France*

[5] *Université Lyon, ENS de Lyon, Universitée Claude Bernard Lyon 1, CNRS, Laboratoire de Physique, F-69342 Lyon, France*

(Received 2 April 2019; revised manuscript received 9 July 2019; published 16 August 2019)

When a signal is injected in a parametric oscillator close enough to its resonance, the oscillator frequency and phase are locked to those of the injected signal. Here we demonstrate two frequency-locking schemes using a Josephson mixer in the parametric down-conversion regime, pumped beyond the parametric oscillation threshold. The circuit then emits radiation out of two spectrally and spatially separated resonators at frequencies determined by the locking schemes that we choose. When we inject the signal close to a resonance, it locks the oscillator emission to the signal frequency by injection locking. When we inject the signal close to the difference of resonances, it locks the oscillator emission by parametric locking. We compare both schemes and investigate the dependence of the parametric locking range on the pump and the injected-signal power. Our results can be interpreted using Adler's theory for lasers, which provides a link between laser physics and superconducting circuits that could enable better understanding of pumped circuits for quantum-information applications such as error correction, circulators, and photon-number detectors.

DOI: 10.1103/PhysRevApplied.12.024034

I. INTRODUCTION

Injection locking is a phenomenon through which the emission frequency and phase of a parametric oscillator become locked to those of an injection tone. It is usually performed by injection of a weak ac signal close to the natural oscillator frequency and has given rise to applications including narrowing of the linewidth of lasers [1,2], driving CMOS-based oscillators [3], understanding synchronization of biological systems [4], and neuromorphic computing [5,6]. Injection locking was recently experimentally realized in various mesoscopic devices [7,8], including micromechanical oscillators [9] and superconducting circuits [10,11].

In this paper we demonstrate parametric locking of two nondegenerate oscillators with resonance frequencies ω_a and ω_b by a signal injected close to the difference of their frequencies $\omega_a - \omega_b$. The oscillators are coupled by a Josephson circuit pumped at $\omega_p = \omega_a + \omega_b$. We show that parametric locking relies on multiphotonic processes occurring in the Josephson circuit and we compare it with the injection locking by a signal injected close to the natural frequency ω_a or ω_b of one of the oscillators. We illustrate the differences between these two approaches by measuring the frequency and power dependence of the emission spectra of the two resonators and describe our observations using an extension of Adler's theory [12].

II. MEASUREMENT SETUP AND DEVICE PARAMETERS

In our devices, resonators a and b are the $\lambda/2$ modes of two aluminum superconducting microstrip lines arranged in a cross shape. They resonate at frequencies $\omega_a = 2\pi \times 8.445$ GHz and $\omega_b = 2\pi \times 6.451$ GHz. They are physically connected in their center by a Josephson ring modulator (JRM; Fig. 1) [13–15], which couples them when their common mode is pumped far from resonance with an external signal of amplitude p. The Hamiltonian of the circuit is then given by

$$\hat{H} = \hbar\omega_a \hat{a}^\dagger \hat{a} + \hbar\omega_b \hat{b}^\dagger \hat{b} + \hat{H}_{\mathrm{JRM}}, \quad (1)$$

*benjamin.huard@ens-lyon.fr

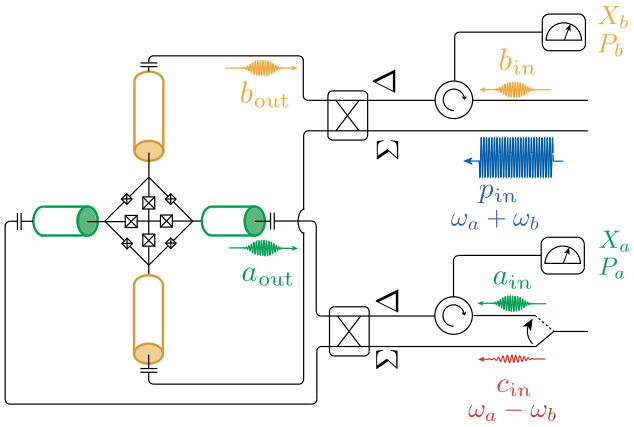

FIG. 1. The Josephson mixer consists of two microwave resonators a (orange) and b (green) resonating at different frequencies ω_a and ω_b that are coupled via a Josephson ring modulator. Two 180° hybrid couplers (circuits in rounded boxes) are used to inject microwave signals in both differential and common driving on a and b ports. The circuit can be pumped at amplitude p_{in} and frequency $\omega_p = \omega_a + \omega_b$ above the parametric oscillation threshold. An additional locking drive is injected on mode a_{in} at frequency $\omega_{\text{in},a} \approx \omega_a$, on mode b_{in} at frequency $\omega_{\text{in},b} \approx \omega_b$, or on the common mode c_{in} at frequency $\omega_c \approx \omega_a - \omega_b$.

where, at the lowest order in the fields, the JRM Hamiltonian reads [13,15]

$$\hat{H}_{\text{JRM}} = \hbar\chi(p + p^*)(\hat{a} + \hat{a}^\dagger)(\hat{b} + \hat{b}^\dagger). \tag{2}$$

When the pump is applied at frequency $\omega_p = \omega_a + \omega_b$, this three-wave-mixing Hamiltonian simplifies to the parametric down-conversion Hamiltonian [15,16] in the rotating-wave approximation as $\hat{H}_{\text{PDC}} = \hbar\chi(p\hat{a}^\dagger\hat{b}^\dagger + p^*\hat{a}\hat{b})$. Two regimes can be distinguished as a function of pump power. Below the so-called parametric oscillation threshold ($p_{\text{in}} < p_{\text{th}}$), the circuit behaves as a nondegenerate amplifier. Without any input drives on a and b ports, the circuit amplifies vacuum fluctuations into the output modes a_{out} and b_{out}. More precisely, it generates a vacuum two-mode squeezed state nondegenerate in frequency and space [17] whose squeezing ratio increases with the pump power. The threshold power corresponds to a conversion rate of pump photons into a and b photons that is as large as the geometric mean of the dissipation rates κ_a and κ_b of modes a and b, such that the cooperativity $C = 4\chi^2|p_{\text{th}}|^2/(\kappa_a\kappa_b)$ is 1. Beyond this threshold, the device enters the parametric oscillation regime characterized by a spontaneous generation of photons in the two resonators and correlated emissions [18] from modes a and b. In the absence of mechanisms limiting the resonators' populations, this regime is unstable as the number of photons keeps increasing. There are typically two processes that can stabilize parametric oscillations. First, the pump power can be depleted as down-conversion becomes stronger, such that the pump cannot be considered stiff anymore and p does not increase with p_{in} any longer. It is this process that usually stabilizes lasing in optics [19,20]. Second, Kerr nonlinearities can shift the mode frequencies when the pump power increases, and they ultimately limit the parametric down-conversion rate [11]. In microwave experiments such as ours, where nonlinearities induced by Josephson junctions are relatively much larger than in optics, the second process dominates the first one and is thus responsible for parametric oscillation stabilization [21].

The Kerr nonlinearities are generally described by an extra term in the Hamiltonian, which can be written in the rotating-wave approximation [22] as

$$\hat{H}_K = \hbar\left[\chi_a(\hat{a}^\dagger)^2\hat{a}^2 + \chi_b(\hat{b}^\dagger)^2\hat{b}^2 + \chi_{ab}\hat{a}^\dagger\hat{a}\hat{b}^\dagger\hat{b}\right], \tag{3}$$

where χ_a and χ_b are self-Kerr-coefficients of the two resonators and $\chi_{ab} = 4\sqrt{\chi_a\chi_b}$ is their cross-Kerr-coefficient. They effectively modify the oscillator frequencies by a detuning $\chi_a(\hat{a}^\dagger\hat{a}) + \chi_{ab}(\hat{b}^\dagger\hat{b})$ for resonator a and $\chi_b(\hat{b}^\dagger\hat{b}) + \chi_{ab}(\hat{a}^\dagger\hat{a})$ for resonator b.

As parametric oscillation is stabilized, the resulting outgoing field amplitudes a_{out} and b_{out} exhibit similar properties as in previously studied spatially degenerate Josephson amplifiers [11,23]. Performing repeated heterodyne quadrature measurements of the outgoing field amplitudes reveals quadrature statistics that is characteristic of parametric oscillation (see Figs. 6 and 7). As previously demonstrated [11], we observe that nondegenerate parametric oscillations occur with an arbitrary phase, as expected from the highly degenerate state of the system.

III. INJECTION LOCKING

The standard approach to suppress phase indeterminacy of parametric oscillations is to use injection locking. It consists in injecting a small signal at the resonance frequency of the oscillator, hence breaking the phase degeneracy of the system. The oscillations lock to the phase of the injected signal, which consequently narrows the linewidth of the emissions. In Fig. 2(a), we show that this usual scheme can be applied to our device by driving mode a at a frequency $\omega_{\text{in},a}$, close to its natural resonance frequency ω_a [Fig. 2(a)]. Here the pump power P_p is fixed to −16 dBm (referred to the input of the dilution refrigerator) so that the cooperativity is set to $C \approx 1$. With a constant input drive power at $\omega_{\text{in},a}$, we measure the spectral noise power $S_a(\omega)$ in the output mode a_{out} as a function of $\omega_{\text{in},a}$. At low-enough detuning $\omega_{\text{in},a} - \omega_a$, a single peak can be seen in the spectrum and is localized at $\omega_{\text{in},a}$ [Fig. 2(a)], hence indicating that the oscillator frequency is pulled by the input tone and gets locked to it. This process works for input frequencies within some injection-locking range $|\omega_{\text{in},a} - \omega_a| < \Delta\omega_{\text{in}}/2$. Beyond that range, the emission

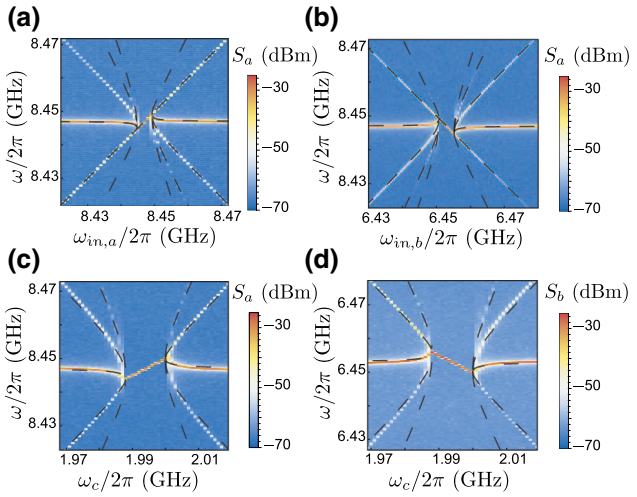

FIG. 2. (a),(b) Measured power spectral density $S_a(\omega)$ emitted into mode a_{out} as a function of emission frequency ω and frequency $\omega_{\text{in},a}$ ($\omega_{\text{in},b}$) of the tone injected on mode a (b). The signal is injected at a fixed power $P_{\text{in}} = -26$ dBm for both mode a and mode b. Dashed black lines correspond to Adler's theory (see the text). (c),(d) Measured power spectral densities $S_a(\omega)$ and $S_b(\omega)$ emitted from modes a_{out} and b_{out} as a function of emission frequency ω and frequency ω_c of the tone injected on the common mode at fixed power $P_c = -26$ dBm. For all measurements the pump frequency ω_p is fixed at $2\pi \times 14.9$ GHz and the pump power P_p is fixed at -16 dBm.

spectrum consists of a series of peaks that match Adler's theory [12] for injection locking since they are localized at

$$\omega_n(\omega_{\text{in},a}) = \omega_{\text{in},a} + (n+1)\omega_{\text{beat}}(\omega_{\text{in},a}) \tag{4}$$

for an arbitrary integer index n, where the beating frequency ω_{beat} is defined as [24]

$$\omega_{\text{beat}}(\omega) = (\omega_a - \omega)\sqrt{1 - \left(\frac{\Delta\omega_{\text{in}}}{2(\omega_a - \omega)}\right)^2}. \tag{5}$$

The resulting frequencies $\omega_n(\omega_{\text{in},a})$, shown as dashed lines in Fig. 2, match precisely with the position of the peaks in the emission spectra of the circuits. The peak corresponding to $n = 0$ corresponds to the pulled oscillator frequency, which becomes equal to its natural frequency when $|\omega_{\text{in},a} - \omega_a| \gg \Delta\omega_{\text{in}}$ and deviates significantly as $\omega_{\text{in},a}$ approaches ω_a. In agreement with the theory, we observe experimentally that ω_0 evolves continuously as we sweep the injection frequency and matches $\omega_{\text{in},a}$ in the injection-locking range. The peak corresponding to $n = -1$ is exactly at the injection frequency for all $\omega_{\text{in},a}$. Other values of n can be observed and correspond to higher-order-frequency-distortion sidebands.

Since for nondegenerate parametric oscillations the phases of the oscillations are correlated in resonators a and b, it is sufficient to inject a signal in only one of them to suppress simultaneously their phase indeterminacy. As a consequence, by injecting a signal at frequency $\omega_{\text{in},b} \approx \omega_b$ in resonator b, we observe the same injection-locking phenomena as before when looking at the emission spectrum of resonator a [Fig. 2(b)]. One striking difference is that, within the injection-locking range, the frequency of the emission peak is given by $\widetilde{\omega}_{\text{in},a} = \omega_p - \omega_{\text{in},b}$ rather than $\omega_{\text{in},a}$, and therefore decreases as we increase the frequency of the injected signal. One advantage of this two-mode injection locking is that the injected signal can be spatially and spectrally separated from the natural frequency of the oscillator. This could be useful for certain applications, where, for example, one of the resonators has to remain isolated such as in a quantum memory [25]. Beyond the locking range, the emission-spectrum frequency peaks are localized at $\omega_n(\widetilde{\omega}_{\text{in},a})$ according to Eq. (4). The measured spectral peaks match well these frequencies [dashed lines in Fig. 2(b)], so their frequencies are also captured by Adler's theory when $\omega_{\text{in},a}$ is replaced by $\omega_p - \omega_{\text{in},b}$.

IV. PARAMETRIC LOCKING

We demonstrate a strategy to suppress phase indeterminacy that relies on what we call "parametric locking" instead of injection locking. Since the sum of the phases of the two modes $\theta_a + \theta_b$ is fixed [21] when the system is pumped at $\omega_a + \omega_b$, one needs only a single extra constraint to determine the phases of the outgoing field unequivocally. This can be obtained by pumping the circuit with a parametric drive close to $\omega_a - \omega_b$, which connects the fields in resonators a and b through conversion processes such that $\theta_a - \theta_b$ becomes a constant [26]. In practice, we drive the common mode of the Josephson mixer [22] at $\omega_p = \omega_a + \omega_b$ with an amplitude p above the parametric oscillation threshold and simultaneously at $\omega_c \approx \omega_a - \omega_b$ with an amplitude c. This simultaneous pumping can be used in other power regimes to realize a circulator [27,28] or to simulate ultrastrong coupling between oscillators [16].

Because of this additional drive at ω_c, the three-wave-mixing Hamiltonian acquires extra terms in the rotating-wave approximation,

$$\hbar\chi(c\hat{a}^\dagger\hat{b} + c^*\hat{a}\hat{b}^\dagger), \tag{6}$$

which account for the conversion of photons between resonators a and b. They result in a parametric locking similar to injection locking within a range $\Delta\omega_c$, in which the frequency of emission is given by $(\omega_p + \omega_c)/2$ instead of $\omega_{\text{in},a}$ for mode a and $(\omega_p - \omega_c)/2$ instead of $\omega_{\text{in},b}$ for mode b. Moreover, beyond this range, the spectrum is also composed of a series of peaks, whose frequencies are properly described by Adler's theory provided that in Eq. (4) we use an effective injection-locking frequency $\widetilde{\omega}_{\text{in},a} = (\omega_p + \omega_c)/2$ for mode a and $\widetilde{\omega}_{\text{in},b} = (\omega_p - \omega_c)/2$ for mode b.

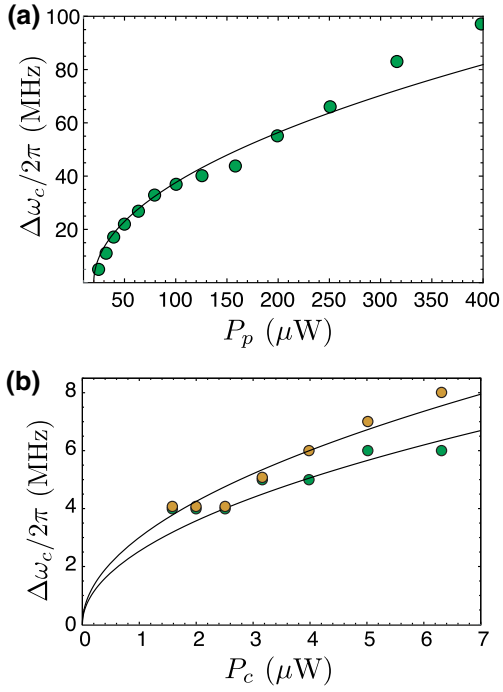

FIG. 3. (a) Parametric locking range $\Delta\omega_c$ measured on resonator a as a function of pump power P_p. The pump frequency ω_p is set to $2\pi \times 14.95$ GHz and the parametric locking tone is injected at ω_c for a constant power $P_c = -20$ dBm. The full black line corresponds to $\Delta\omega_c \propto \sqrt{P_p}$. (b) Parametric locking range measured on the mode a (green dots) and mode b (orange dots) as a function of locking signal power P_c at ω_c. The pump frequency ω_p is set to $2\pi \times 14.95$ GHz and the pump power P_p is set to -16 dBm. Full black lines correspond to $\Delta\omega_c \propto \sqrt{P_c}$.

This behavior is shown in Figs. 2(c) and 2(d), where we have measured power spectral densities $S_a(\omega)$ and $S_b(\omega)$ of the radiation emitted from modes a_{out} and b_{out}, respectively, as a function of the frequency ω_c of the parametric drive. The spectra obtained by parametric locking are similar to those obtained by injection locking [Figs. 2(a) and 2(b)]. However, a couple of striking differences can be observed. Since the effective locking frequency is now given by $(\omega_p \pm \omega_c)/2$, the frequency of the emission peak within the locking range shows a slope $\pm\frac{1}{2}$ as a function of ω_c for modes a and b, respectively. This technique of parametric locking allows us to suppress phase indeterminacy by using only tones that are far from the resonant frequencies of the oscillators. This procedure could be useful for certain applications when one wants the locking signal to remain far from the spectral range of interest. It could also be used in situations where two oscillators are almost degenerate in frequency but outside the technically accessible frequency range. Outside the locking range, the emission-peak frequencies are properly described by Adler's theory with the effective locking frequencies [dashed lines in Figs. 2(c) and 2(d)].

Parametric locking can be made to operate over a larger frequency range by increasing the pump power P_p at ω_p away from the parametric oscillation threshold. It can be shown using Langevin equations (see Appendix A) that at low pump powers we expect $\Delta\omega_c$ to be proportional to the pump amplitude $|p|$ and thus to $\sqrt{P_p}$. This is another qualitative difference compared with the case of injection locking, where $\Delta\omega_{\text{in}}$ is proportional to $\sqrt{|p|}$ and thus to $P_p^{1/4}$. As shown in Fig. 3(a), we observe that the size of the locking range indeed follows the expected behavior as a function of pump power. At larger pump power P_p, higher-order terms start to contribute significantly and the locking range has a more-complex evolution.

We also observe a power dependence of the parametric locking range with the power of the injected parametric signal. It is well known for standard injection locking [8] that the locking range is proportional to the amplitude of the injected signal and is therefore a square-root function of the injected power P_{in} as predicted by Adler's theory. We observe that for parametric locking the locking range increases similarly with the strength of the injected parametric signal [Fig. 3(b)], suggesting that a stronger injected signal is favorable to suppress phase indeterminacy in resonators a and b. For these measurements as well as those in Fig. 2, the injected-signal powers are chosen so that the frequency of the peak in the middle of the locking range is the same for all experiments to ease comparisons.

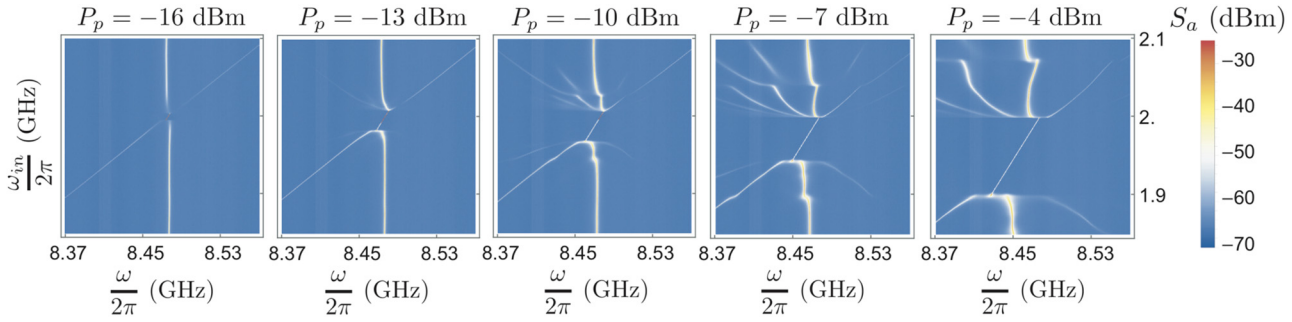

FIG. 4. Measured power spectral density $S_a(\omega)$ of mode a_{out} as a function of ω and ω_c for different pump powers P_p. The pump frequency ω_p is set to $2\pi \times 14.952$ GHz and the locking signal is injected at a constant power $P_c = -20$ dBm.

Finally, we explore the parametric locking behavior of our circuit well beyond the parametric threshold by increasing the pump power P_p. This reveals qualitative deviations from Adler's theory as can be seen in the measured spectra in Fig. 4. At pump powers $P_p > -10$ dBm (referred to the input of the dilution refrigerator), bifurcationlike features [29] appear in the emission-peak frequency dependence due to the importance of microscopic multiphotonic processes involving more than three photons. These features are reminiscent of chaotic behavior [30] and should be studied further.

V. CONCLUSION

We demonstrate injection-locking and parametric locking techniques for coupled nonlinear oscillators that make use of a three-wave-mixing interaction. The geometry of the Josephson circuit we use, based on two spatially and spectrally separated resonators, provides original approaches to suppress the inherent phase indeterminacy of parametric oscillators and lock the field emitted from the resonators. These techniques could be useful for applications in which standard injection locking is not possible. This work illustrates how the strong coupling of superconducting circuits to microwave modes enables the design and use of a variety of nonlinear effects that will be instrumental for quantum-information applications such as quantum error correction, nonreciprocal devices, and detectors.

ACKNOWLEDGMENTS

We thank Zaki Leghtas, Ananda Roy, Thierry Dauxois, the Quantronics group, and Michel Devoret for fruitful interactions over the course of this project. Nanofabrication was done within the consortium Salle Blanche Paris Centre. This work was supported by the EMERGENCES grant QUMOTEL of Ville de Paris and by the French Agence Nationale de la Recherche (GEARED Project No. ANR-14-CE26-0018).

APPENDIX A: PARAMETRIC OSCILLATION

In our experiment, we measure emission spectra of a Josephson circuit in the parametric oscillation regime. The circuit is driven by a pump at an amplitude larger than the amplitudes used in the linear parametric amplification regime. The threshold pump amplitude is defined by cooperativity C equal to 1 and is thus given by $|\chi p_{\mathrm{th}}|^2 = \kappa_a\kappa_b/4$.

We detect the threshold by measuring the distribution of the field quadratures for different pump amplitudes. The signal emitted from mode a (b) is amplified and its two quadratures X_a and P_a (X_b and P_b) are determined by heterodyne measurement. In practice, the signals emitted from modes a and b are amplified and mixed with an external local oscillator with a small (few tens of megahertz) detuning $\delta\omega$ from the mode frequencies. The output voltage of the mixer is then digitized with a 250-MHz-bandwidth acquisition board. We demodulate the signals at $\delta\omega$ over a finite time window to determine the two quadratures X and P. It is possible to calibrate these quadratures in meaningful units. If a coherent state $|\alpha\rangle$ is stabilized in mode a, the calibration is such that, on average, $\langle X_a\rangle = \mathrm{Re}\alpha$ and $\langle P_a\rangle = \mathrm{Im}\alpha$. With this choice, the quadratures X and P are dimensionless.

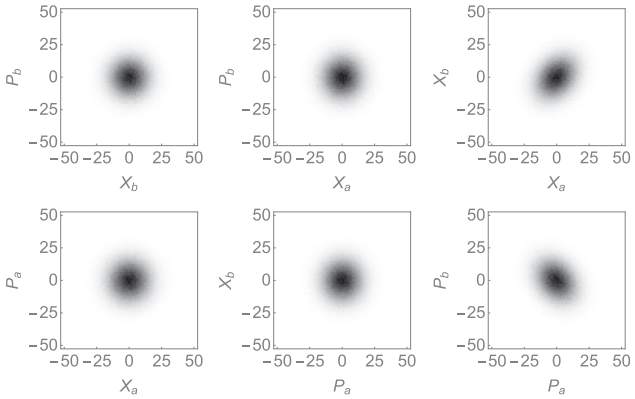

FIG. 5. Field-quadrature histograms of the output fields measured in the linear amplification regime. They correspond to the emission of a two-mode squeezed state by amplification of vacuum fluctuations, as can be inferred from the histograms shown along quadratures of different modes (see Ref. [25] for details).

In the parametric amplification regime, when modes a and b are not driven, the output field is described by a Gaussian distribution centered at the origin. The variance of a single mode a or b is that of the vacuum fluctuations amplified by the Josephson mixer and with the thermal noise added by the chain of amplifiers, as shown in Fig. 5. The apparent two-mode squeezing in the X_a–X_b and

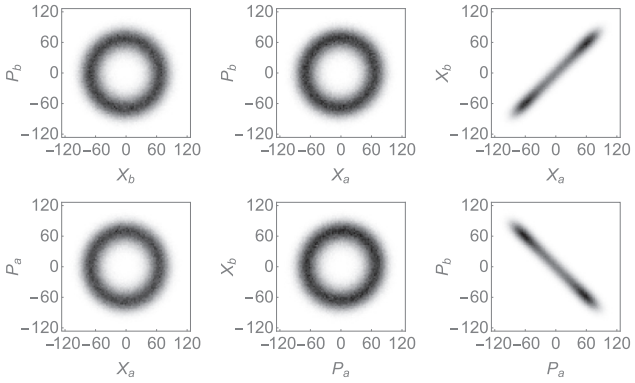

FIG. 6. Distribution of measurement outcomes in the parametric self-oscillation regime for cooperativity $C = 1.3$. The phase of the pump is tuned such that strong correlations are visible in the X_a–X_b and P_a–P_b planes.

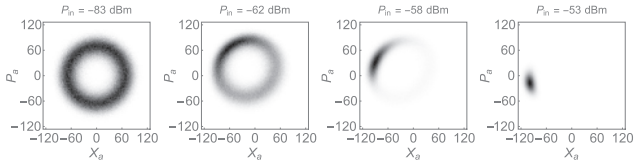

FIG. 7. Measured quadrature statistics for mode a for the pump power fixed in the self-oscillation regime and for four different powers of the small signal injected on resonance into mode a. Field-quadrature axes are calibrated in the square root of the number of photons.

P_a–P_b histograms originates from the vacuum two-mode squeezed state emitted by the device [17].

Beyond the threshold, the self-sustained parametric oscillation state is characterized by complex amplitudes given by

$$a = a_0 e^{i\theta_a},$$
$$b = b_0 e^{i\theta_b}$$

and highly degenerate phases θ_a and θ_b of the fields [11]. This regime is shown in Fig. 6. While a minimum of potential energy is reached for any phase θ_a or θ_b, the sum of the phases is constrained and given by the phase of the pump up to an offset that depends on cooperativity. In Fig. 6, we chose the phase of the pump to highlight this phase constraint in the X_a–X_b and P_a–P_b phase spaces.

We then inject a weak tone at frequency ω_{in} on resonance in mode a and measure the quadrature statistics for different powers of the injected signal. The histograms shown in Fig. 7 demonstrate the transition from the phase-unlocked regime to the phase-locked regime. A global rotation from one histogram to the next corresponds to a slowly drifting phase in the detection setup.

APPENDIX B: INJECTION-LOCKING AND PARAMETRIC LOCKING RANGE CALCULATED USING THE LANGEVIN-EQUATION FORMALISM

1. Injection locking

When the circuit is pumped at $\omega_p = \omega_a + \omega_b$, it can be described by the classical Langevin equations

$$\begin{aligned}\frac{da}{dt} &= -i\omega_a a - i\chi p b^* - \Gamma_a a + i\chi_a |a|^2 a \\ &\quad + i\chi_{ab}|b|^2 a + \sqrt{2\Gamma_a}a_{\text{in}}, \\ \frac{db}{dt} &= -i\omega_b b - i\chi p a^* - \Gamma_b b + i\chi_b |b|^2 b \\ &\quad + i\chi_{ab}|a|^2 b + \sqrt{2\Gamma_b}b_{\text{in}},\end{aligned} \tag{B1}$$

where $\Gamma_a = \kappa_a/2$, $\Gamma_b = \kappa_b/2$, where κ_a and κ_b are the dissipation rates of the modes of amplitude a and b, and $p = |p|e^{-i\omega_p t}$ is the amplitude of the pump applied on the common mode. We include fourth-order Kerr terms necessary for the stabilization of parametric oscillation.

On top of these equations, the fields, which can have complex amplitudes, obey the following boundary conditions:

$$\begin{aligned}\sqrt{2\Gamma_a}a &= a_{\text{in}} + a_{\text{out}}, \\ \sqrt{2\Gamma_b}b &= b_{\text{in}} + b_{\text{out}}\end{aligned}. \tag{B2}$$

In the parametric oscillation regime and beyond threshold, the number of photons grows rapidly in the resonators ($n_a \gg 1$ and $n_b \gg 1$), such that the outgoing power is much larger than the incoming power. We then have $\sqrt{2\Gamma_a}a \approx a_{\text{out}}$ and $\sqrt{2\Gamma_b}b \approx b_{\text{out}}$. Because of energy conservation, the number of outgoing photons must be the same for resonators a and b, and therefore $|a_{\text{out}}| \approx |b_{\text{out}}|$. It is therefore straightforward to show that

$$\Gamma_a n_a \approx \Gamma_b n_b \tag{B3}$$

if $n_a = |a|^2$ and $n_b = |b|^2$ are the numbers of photons in each mode.

For injection locking to occur, one injects a small signal $a_{\text{in}} = |a_{\text{in}}|e^{-i\omega t}$ in resonator a, whereas $b_{\text{in}} = 0$, such that the fields a and b acquire well-defined phases and frequencies. We can therefore write $a = \tilde{a}e^{-i\omega t}$ and $b = \tilde{b}e^{-i(\omega_p-\omega)t}$, where the complex amplitudes $\tilde{a}$ and $\tilde{b}$ do not depend on time. Using these expressions in Eq. (B1), we find the following expression for the field in resonator a:

$$a = \frac{\sqrt{2\Gamma_a}a_{\text{in}}}{-i\left(\Delta\omega + \chi_a n_a + \chi_{ab}n_b\right) + \Gamma_a - \frac{|\chi p|^2}{i(-\Delta\omega + \chi_b n_b + \chi_{ab}n_a) + \Gamma_b}}, \tag{B4}$$

where we have defined $\Delta\omega = \omega - \omega_a$.

For a large field to arise in the resonator ($|a| \gg 1$) when a vanishing injection-tone amplitude $|a_{\text{in}}| \to 0$ is applied, the denominator of the previous expression must become smaller than $\sqrt{\Gamma_a}|a_{\text{in}}|$. Therefore, when injection locking happens, one can write

$$\begin{aligned}&[-i\left(\Delta\omega + \chi_a n_a + \chi_{ab}n_b\right) + \Gamma_a] \\ &\quad \times [i\left(-\Delta\omega + \chi_b n_b + \chi_{ab}n_a\right) + \Gamma_b] - |\chi p|^2 \to 0.\end{aligned} \tag{B5}$$

The real part of this expression gives the condition for injection locking to occur,

$$\begin{aligned}|\chi p|^2 &\approx \Gamma_a\Gamma_b + (\Delta\omega + \chi_a n_a + \chi_{ab}n_b) \\ &\quad \times (-\Delta\omega + \chi_b n_b + \chi_{ab}n_a),\end{aligned} \tag{B6}$$

while the imaginary part gives the relation between the number of photons and the frequency shift with respect to

the natural frequency of the oscillator,

$$\Gamma_b(\Delta\omega + \chi_a n_a + \chi_{ab} n_b) \approx \Gamma_a(-\Delta\omega + \chi_b n_b + \chi_{ab} n_a). \tag{B7}$$

Using the condition (B3) that $\Gamma_a n_a \approx \Gamma_b n_b$, one obtains from Eqs. (B6) and (B7)

$$|\chi p|^2 = \Gamma_a\Gamma_b + (\Delta\omega + \tilde{\chi}_a n_a)(-\Delta\omega + \tilde{\chi}_b n_a) \tag{B8}$$

and

$$\Gamma_b(\Delta\omega + \tilde{\chi}_a n_a) = \Gamma_a(-\Delta\omega + \tilde{\chi}_b n_a), \tag{B9}$$

respectively, where we have defined $\tilde{\chi}_a = \chi_a + \chi_{ab}\Gamma_a/\Gamma_b$ and $\tilde{\chi}_b = \chi_{ab} + \chi_b\Gamma_a/\Gamma_b$. Equations (B8) and (B9) have a single solution $(\Delta\omega_0, n_{a0})$, which means that the frequency range over which the locking can occur is infinitely small $(\Delta\omega_{\text{in}} = \Delta\omega_{\max} - \Delta\omega_{\min} \approx 0)$.

For larger injection-tone amplitude (i.e., $|a_{\text{in}}| \sim \sqrt{\Gamma_a}$) but still under the condition $\Gamma_a n_a \gg |a_{\text{in}}|^2$, the square modulus of Eq. (B4) combined with Eq. (B3) gives

$$n_a = \left| \frac{\sqrt{2\Gamma_a}a_{\text{in}}}{-i\,(\Delta\omega + \tilde{\chi}_a n_a) + \Gamma_a + \frac{|\chi p|^2}{i(-\Delta\omega + \tilde{\chi}_b n_a) + \Gamma_b}} \right|^2, \tag{B10}$$

which has an ensemble of solutions forming an ellipselike shape centered at $(\Delta\omega_0, n_{a0})$ in the $\{\Delta\omega, n_a\}$ phase space, and whose major axis is given by Eq. (B8). We can therefore find an approximate expression for the maximum and minimum frequency shift $\Delta\omega$ along this axis by combining Eqs. (B10) and (B8). This leads to

$$\begin{aligned} &n_a \times [\Gamma_b(\Delta\omega + \tilde{\chi}_a n_a) - \Gamma_a(-\Delta\omega + \tilde{\chi}_b n_a)]^2 \\ &\quad = 2\Gamma_a|a_{\text{in}}|^2\left[\Gamma_b^2 + (\Delta\omega - \tilde{\chi}_b n_a)^2\right], \end{aligned} \tag{B11}$$

and then by introducing $\delta\omega = \Delta\omega - \Delta\omega_0$ and $\delta n_a = n_a - n_{a0}$, we obtain the relation between the resonator population δn_a for an injection amplitude a_{in} and the frequency shift $\delta\omega$:

$$\begin{aligned} &n_a \times [\Gamma_b(\delta\omega + \tilde{\chi}_a \delta n_a) - \Gamma_a(-\delta\omega + \tilde{\chi}_b \delta n_a)]^2 \\ &\quad = 2\Gamma_a|a_{\text{in}}|^2\left[\Gamma_b^2 + (\Delta\omega - \tilde{\chi}_b n_a)^2\right], \end{aligned} \tag{B12}$$

where we have used the fact that $(\Delta\omega_0, n_{a0})$ is the solution of Eq. (B9).

Equation (B12) can be simplified by introducing the three constants

$$\begin{aligned} \alpha &= (\Gamma_a + \Gamma_b) + (\Gamma_b\tilde{\chi}_a - \Gamma_a\tilde{\chi}_b) \\ &\quad \times \frac{2\Delta\omega_0 - (\tilde{\chi}_b - \tilde{\chi}_a)n_{a0}}{(\tilde{\chi}_b - \tilde{\chi}_a)\Delta\omega_0 + 2\tilde{\chi}_a\tilde{\chi}_b n_{a0}}, \\ \beta &= \frac{\tilde{\chi}_b\Gamma_a - \tilde{\chi}_a\Gamma_b}{\Gamma_a + \Gamma_b} - \tilde{\chi}_b, \\ \gamma &= \left|\frac{\Gamma_a + \Gamma_b}{\tilde{\chi}_a + \tilde{\chi}_b}\right| \times \sqrt{\frac{1}{\Gamma_a\Gamma_b}}, \end{aligned} \tag{B13}$$

which linearly relate $\delta\omega$ to δn_a, $\Delta\omega_0$ to n_{a0}, and n_{a0} to $|\chi p|$ in the following way

$$\begin{aligned} &\Gamma_b(\delta\omega + \tilde{\chi}_a\delta n_a) - \Gamma_a(-\delta\omega + \tilde{\chi}_b\delta n_a) = \alpha \times \delta\omega, \\ &\Delta\omega_0 - \tilde{\chi}_b n_{a0} = \beta \times n_{a0}, \\ &n_{a0} = \gamma \times |\chi p|\,, \end{aligned} \tag{B14}$$

given that the number of photons in the resonator remains very large ($\Gamma_a\Gamma_b \ll |\chi p|^2$ and $\Gamma_b \ll \tilde{\chi}_b n_a$). The constants β and γ are obtained using the fact that $(\Delta\omega_0, n_{a0})$ is the the solution of Eqs. (B8) and (B9), while α is obtained by linearization of Eq. (B8) to the first order in $\delta\omega$ and δn_a.

At the lowest order in $\delta\omega$, δn_a, and $|a_{\text{in}}|$ and for $\Gamma_b \ll \tilde{\chi}_a n_{a0}$, Eq. (B12) then becomes

$$\gamma \times |\chi p|\,\alpha^2\delta\omega^2 = 2\Gamma_a|a_{\text{in}}|^2\beta^2(\gamma \times |\chi p|)^2, \tag{B15}$$

which gives two symmetric solutions $\pm\delta\omega$ such that the locking range $\Delta\omega_{\text{in}} = 2\delta\omega$ is given by

$$\Delta\omega_{\text{in}} \approx 2\sqrt{2\Gamma_a}\sqrt{\frac{\beta^2\gamma}{\alpha^2}}|a_{\text{in}}|\sqrt{|\chi p|}. \tag{B16}$$

Expression (B16) shows that the locking range increases as the square root of the injected power $\sqrt{P_{\text{in}}} = |a_{\text{in}}|$ and follows a power law with the pump power $\sqrt{|p|} = P_p^{1/4}$ as mentioned in Fig. 3.

2. Parametric locking

In the case of parametric locking, the circuit is simultaneously pumped at $\omega_p = \omega_a + \omega_b$ and $\omega_c = \omega_a - \omega_b$, and $a_{\text{in}} = b_{\text{in}} = 0$. The Langevin equations thus read

$$\begin{aligned} \frac{da}{dt} &= -i\omega_a a - i\chi p b^* - \Gamma_a a \\ &\quad + i\chi_a|a|^2 a + i\chi_{ab}|b|^2 a - i\chi c b, \\ \frac{db}{dt} &= -i\omega_b b - i\chi p a^* - \Gamma_b b \\ &\quad + i\chi_b|b|^2 b + i\chi_{ab}|a|^2 b - i\chi c^* a, \end{aligned} \tag{B17}$$

where $p = |p|e^{-i(\omega_p t+\varphi_p)}$ and $c = |c|e^{-i(\omega_c t+\varphi_c)}$ are amplitudes of the stiff pumps applied to the common mode of the circuit.

The solutions for which parametric locking occurs can be written as before as $a = \tilde{a}e^{-i\omega_1 t}$ and $b = \tilde{b}e^{-i\omega_2 t}$. Stationary solutions, where $\tilde{a}$ and $\tilde{b}$ do not depend on time, exist only if

$$\omega_1 = \frac{\omega_p + \omega_c}{2} \quad \text{and} \quad \omega_2 = \frac{\omega_p - \omega_c}{2}. \tag{B18}$$

Injecting these solutions into the Langevin equations leads straightforwardly to the expression

$$\frac{a}{a^*} = \frac{2i\chi^2 pc\,(\Delta\omega - \tilde{\chi}_b n_a) \,/\, \left[(\Delta\omega - \tilde{\chi}_b n_a)^2 + \Gamma_b^2\right]}{-i\Delta\omega + \Gamma_a - i\tilde{\chi}_a n_a - \frac{|\chi p|^2}{\Gamma_b - i(\Delta\omega - \tilde{\chi}_b n_a)} + \frac{|\chi c|^2}{\Gamma_b + i(\Delta\omega - \tilde{\chi}_b n_a)}}, \tag{B19}$$

where we have taken $\omega_1 = \omega$ and $\omega_2 = \omega_p - \omega$ and define $\Delta\omega = \omega - \omega_a$.

Similarly to injection locking in the case of vanishing input amplitude a_{in}, this expression has a single solution $(\Delta\omega_0, n_{a0})$ if $c \to 0$.

For a finite pump amplitude c, the solutions also form an ellipse in the $\{\Delta\omega, n_a\}$ phase space, whose center is given by $(\Delta\omega_0, n_{a0})$ and whose major axis is given by the solution of Eq. (B8). Similarly to injection locking, we can find an approximate expression for the maximum and minimum frequency shifts $\Delta\omega$ along this axis by combining Eqs. (B8) and (B19) and using the fact that in the experiment $|p| \gg |c|$ and that the numbers of photons n_a and n_b are large. Equation (B19) thus simplifies to

$$\frac{a}{a^*} \approx \frac{i2\chi^2 pc}{\alpha\delta\omega}, \tag{B20}$$

where α is the same constant as for injection locking and $\delta\omega = \Delta\omega - \Delta\omega_0$.

We thus find the parametric locking range to be

$$\Delta\omega_c = 4\chi^2 \frac{|pc|}{\alpha}, \tag{B21}$$

which shows that the locking range increases as $\sqrt{P_p}$ and $\sqrt{P_c}$. The two pumps therefore act in a similar way for parametric locking.

[1] H. L. Stover and W. H. Steier, Locking of laser oscillators by light injection, App. Phys. Lett. **8**, 91 (1966).

[2] J. Hillbrand, A. M. Andrews, H. Detz, G. Strasser, and B. Schwarz, Coherent injection locking of quantum cascade laser frequency combs, Nat. Photonics **13**, 101 (2019).

[3] B. Razavi, A study of injection locking and pulling in oscillators, IEEE J. Solid-State Circuits **39**, 1415 (2004).

[4] R. E. Mirollo and S. H. Strogatz, Synchronization of pulse-coupled biological oscillators, SIAM J. Appl. Math. **50**, 1645 (1990).

[5] M. Romera, P. Talatchian, S. Tsunegi, F. A. Araujo, V. Cros, P. Bortolotti, K. Yakushiji, A. Fukushima, H. Kubota, S. Yuasa, D. Vodenicarevic, N. Locatelli, D. Querlioz, and J. Grollier, Vowel recognition with four coupled spin-torque nano-oscillators, Nature **563**, 230 (2018).

[6] D. Marković, N. Leroux, M. Riou, F. Abreu Araujo, J. Torrejon, D. Querlioz, A. Fukushima, S. Yasa, J. Trastoy, P. Bortolotti, and J. Grollier, Reservoir computing with the frequency, phase, and amplitude of spin-torque nano-oscillators, App. Phys. Lett. **114**, 012409 (2019).

[7] W. H. Rippard, M. R. Pufall, S. Kaka, T. J. Silva, S. E. Russek, and J. A. Katine, Injection Locking and Phase Control of Spin Transfer Nano-oscillators, Phys. Rev. Lett. **95**, 067203 (2005).

[8] Y. Liu, J. Stehlik, M. J. Gullans, J. M. Taylor, and J. R. Petta, Injection locking of a semiconductor double-quantum-dot micromaser, Phys. Rev. A **92**, 053802 (2015).

[9] M. Zhang, G. S. Wiederhecker, S. Manipatruni, A. Barnard, P. Mceuen, and M. Lipson, Synchronization of Micromechanical Oscillators Using Light, Phys. Rev. Lett. **109**, 233906 (2012).

[10] M. C. Cassidy, A. Bruno, S. Rubbert, M. Irfan, J. Kammhuber, R. N. Schouten, A. R. Akhmerov, and L. P. Kouwenhoven, Demonstration of an ac josephson junction laser, Science **355**, 939 (2017).

[11] A. Bengtsson, P. Krantz, M. Simoen, I. M. Svensson, B. Schneider, V. Shumeiko, P. Delsing, and J. Bylander, Nondegenerate parametric oscillations in a tunable superconducting resonator, Phys. Rev. B **97**, 144502 (2018).

[12] R. Adler, Locking phenomena in oscillators, Proc. IEEE **61**, 10 (1973).

[13] N. Bergeal, F. Schackert, M. Metcalfe, R. Vijay, V. E. Manucharyan, L. Frunzio, D. E. Prober, R. J. Schoelkopf, S. M. Girvin, and M. H. Devoret, Phase-preserving amplification near the quantum limit with a josephson ring modulator, Nature **465**, 64 (2010).

[14] N. Roch, E. Flurin, F. Nguyen, P. Morfin, P. Campagne-Ibarcq, M. H. Devoret, and B. Huard, Widely Tunable, Nondegenerate Three-wave Mixing Microwave Device Operating near the Quantum Limit, Phys. Rev. Lett. **108**, 147701 (2012).

[15] B. Abdo, A. Kamal, and M. Devoret, Nondegenerate three-wave mixing with the josephson ring modulator, Phys. Rev. B **87**, 014508 (2013).

[16] D. Marković, S. Jezouin, Q. Ficheux, S. Fedortchenko, S. Felicetti, T. Coudreau, P. Milman, Z. Leghtas, and B. Huard, Demonstration of an Effective Ultrastrong Coupling between two Oscillators, Phys. Rev. Lett. **121**, 040505 (2018).

[17] E. Flurin, N. Roch, F. Mallet, M. H. Devoret, and B. Huard, Generating Entangled Microwave Radiation Over two Transmission Lines, Phys. Rev. Lett. **109**, 183901 (2012).

[18] A. Kamal, A. Marblestone, and M. Devoret, Signal-to-pump back action and self-oscillation in double-pump

josephson parametric amplifier, Phys. Rev. B **79**, 184301 (2009).
[19] S. Reynaud, C. Fabre, and E. Giacobino, Quantum fluctuations in a two-mode parametric oscillator, J. Opt. Soc. Am. B **4**, 1520 (1987).
[20] D. F. Walls and G. J. Milburn, *Quantum Optics* (Springer, Berlin, 2008).
[21] W. Wustmann and V. Shumeiko, Nondegenerate parametric resonance in a tunable superconducting cavity, Phys. Rev. App. **8**, 024018 (2017).
[22] E. Flurin, Ph.D. thesis, École Normale Supérieure, Paris, 2014.
[23] C. M. Wilson, T. Duty, M. Sandberg, F. Persson, V. Shumeiko, and P. Delsing, Photon Generation in an Electromagnetic Cavity with a Time-dependent Boundary, Phys. Rev. Lett. **105**, 233907 (2010).
[24] M. Armand, On the spectrum of the unlocked driven oscillators, Proc. IEEE **57**, 798 (1969).
[25] E. Flurin, N. Roch, J. D. Pillet, F. Mallet, and B. Huard, Superconducting Quantum Node for Entanglement and Storage of Microwave Radiation, Phys. Rev. Lett. **114**, 090503 (2015).
[26] B. Abdo, K. Sliwa, F. Schackert, N. Bergeal, M. Hatridge, L. Frunzio, A. D. Stone, and M. Devoret, Full Coherent Frequency Conversion between two Propagating Microwave Modes, Phys. Rev. Lett. **110**, 173902 (2013).
[27] K. M. Sliwa, M. Hatridge, A. Narla, S. Shankar, L. Frunzio, R. J. Schoelkopf, and M. H. Devoret, Reconfigurable Josephson Circulator / Directional Amplifier, Phys. Rev. X **5**, 041020 (2015).
[28] T.-C. Chien, O. Lanes, C. Liu, X. Cao, P. Lu, S. Motz, G. Liu, D. Pekker, and M. Hatridge, Multiparametric amplification and qubit measurement with a Kerr-free Josephson ring modulator, arXiv:1903.02102 (2019).
[29] C. Richy, K. I. Petsas, E. Giacobino, C. Fabre, and L. Lugiato, Observation of bistability and delayed bifurcation in a triply resonant optical parametric oscillator, J. Opt. Soc. Am. B **12**, 456 (1995).
[30] L. A. Lugiato, C. Oldano, C. Fabre, E. Giacobino, and R. J. Horowicz, Bistability, self-pulsing and chaos in optical parametric oscillators, Nuovo Cimento D **10**, 959 (1988).